Quart. J. R. Met. Soc. (1983), **109**, pp. 549–564

551.553.1:551.558.4(56)

A study of meteorological patterns associated with a lake confined by mountains – the Dead Sea case

By M. SEGAL*, Y. MAHRER** and R. A. PIELKE*

* *Department of Atmospheric Science, Colorado State University, Fort Collins, Colorado 80523*

** *Department of Soil and Water Sciences, The Hebrew University of Jerusalem, Rehovot, Israel*

(Received 13 May 1982, revised 12 January 1983. Communicated by Professor W. M. Gray)

SUMMARY

A planned project to generate hydroelectric power by carrying Mediterranean water into the Dead Sea has stimulated a preliminary numerical model study of the regional meteorological patterns and the evaluation of some possible local climatic modifications. Predicted mesoscale meteorological patterns associated with two frequent synoptic conditions over the region are presented. Emphasis has been focussed on illustrating and studying two general aspects of the thermal circulations generated by a lake which is confined between mountains (LMC): the effect of external flows on the LMC structure and the effects of lake water temperature on the LMC intensity.

1. INTRODUCTION

Numerical model studies of thermally induced circulations due to lakes have been focussed mostly on lakes located in flat terrain (usually with lake sizes of tens of kilometres), e.g. Moroz (1967), Neumann and Mahrer (1975), Physick (1976), Estoque and Gross (1981). In nature, however, numerous lakes are located in mountainous areas (often confined by steep terrain), where much more involved circulation patterns are induced. Numerical model studies by Mahrer and Pielke (1977), Dalu (1978), Ookouchi *et al.* (1978) and Carpenter (1979), which included a mountain ridge adjacent to a large water body, have provided initial modelling insight for such types of terrain combinations. Recent studies by Alpert (1980) and Segal *et al.* (1982a) have considered relatively small lakes confined by mountains; however, a relatively coarse grid resolution was used over the lake region.

A proposed project of constructing a channel to carry water from the Mediterranean Sea to the Dead Sea to generate hydroelectric power (e.g. Weiner 1980) has motivated the model analysis presented in this paper. One focus of the study is to evaluate some of the present meteorological patterns over the region, and to estimate possible changes due to flooding of the Dead Sea with much less saline Mediterranean water. Additionally, it provides an opportunity for further meteorological evaluations of mesoscale circulations generated by a lake confined within a mountainous region. The present paper addresses these aspects (mostly focussing on flow patterns) by simulating two frequent synoptic situations over this region, referred to as: (1) summer day; (2) calm winter day. Emphasis has been placed on studying the following features:

(i) The influence of the synoptic and external mesoscale flows on the combined lake–mountain thermally induced circulations (LMC).

(ii) The effect of the lake surface water temperature on the LMC.

2. CHARACTERISTICS OF THE DEAD SEA

The Dead Sea is located at the bottom of the Jordan Rift Valley (JRV), about 400 m below MSL (Fig. 1). Generally, the lake has an axially symmetric shape for most of its 75 km length, with a typical width of about 15 km. Both longitudinal shores are confined by relatively steep mountainous slopes: the Judean mountains to the west and the Amman plateau to the east, with general top elevations of about 800 m.

The lake water depth varies from several hundred metres in the north to several metres in the southern lake region, causing a non-uniform horizontal distribution of surface water temperatures (Ashbel 1939; Neev and Emery 1967) (in the current study, an

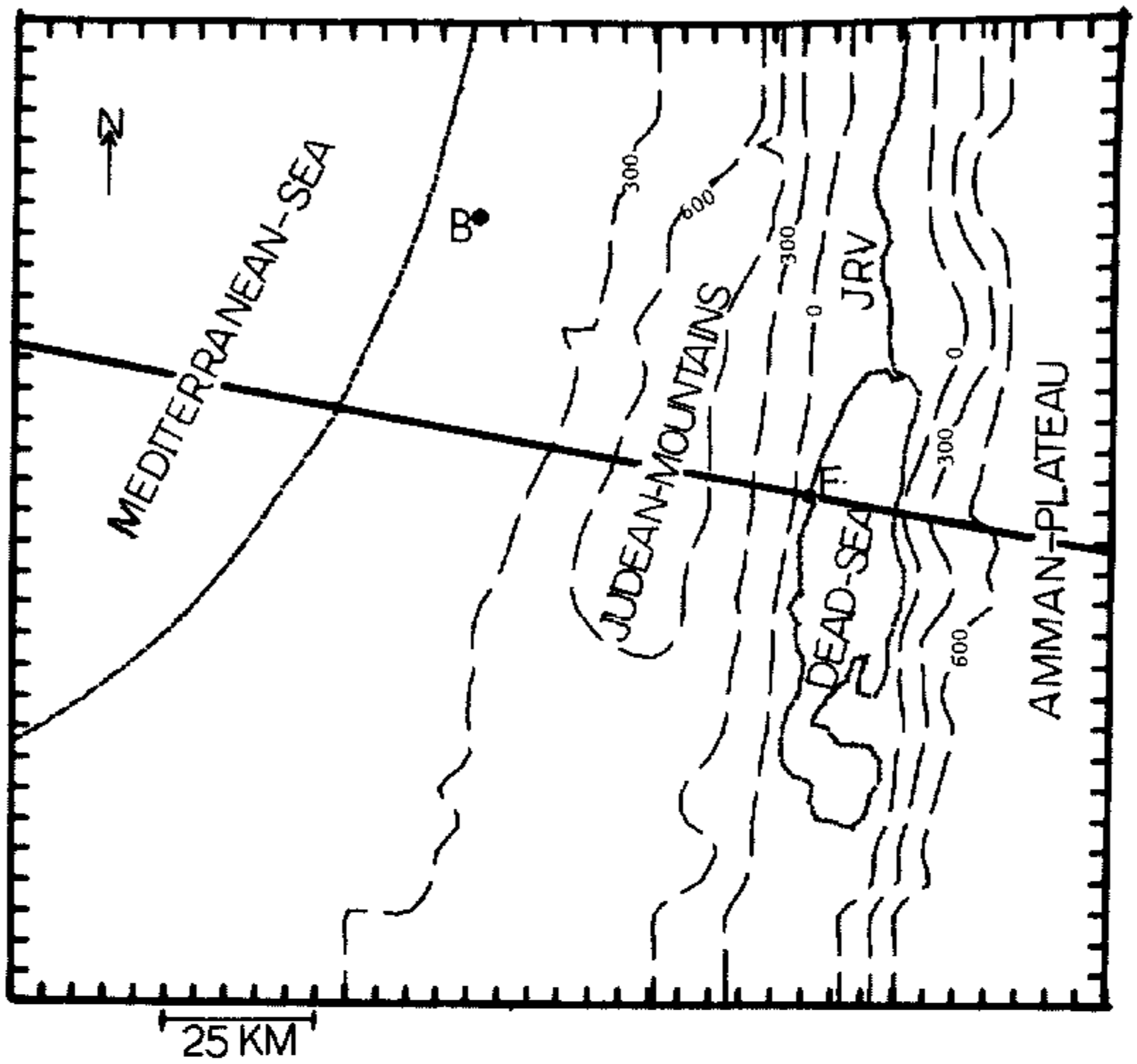

Figure 1. Schematic illustration of the simulated region.

average uniform surface temperature representation over the lake has been adopted as input). The salinity of the lake is about 23%, resulting in some reduction in the evaporation rate from that which would occur if the water were fresh.

Several observationally oriented studies have been carried out for the Dead Sea area, evaluating mostly the summer surface meteorological patterns, excluding, however, the eastern coast of the lake and the water area (e.g. Ashbel 1939; Bitan 1974, 1977). Data from these studies have been used for some model verifications in the current study. Studies by Skibin and Hod (1979) and Doron (1979) of the summer flow patterns in the larger Dead Sea area have provided additional data sources for evaluation.

3. The numerical model

A numerical mesoscale model, whose formulation is given in Pielke (1974) and Mahrer and Pielke (1978), has been used in the present simulations. Simulations were carried out with both two-dimensional (2D) and three-dimensional (3D) model versions, using a 5 km grid interval and 14 vertical levels where the model top is at 7 km above MSL. The 2D simulations (the heavy line in Fig. 1 indicates the simulated cross-section location, while a schematic illustration of the cross-section terrain is given in Fig. 2) consisted, however, of telescoped horizontal grid intervals with 2·5 km lengths over the Dead Sea regions as illustrated by the darker line in Fig. 2. The cubic spline interpolation scheme which is used for the computation of the horizontal advective terms, yielded smooth behaviour of the meteorological fields at the interface of both grids (MacPherson and Kelly (1976) report the success of such a methodology in large-scale simulations). The use of a 2D version is based on the general two-dimensional symmetry of the terrain over a considerable portion of the domain, as well as the desire to have a fine spatial resolution in the vicinity of the lake. The 3D model version with the coarser grid, on the other hand,

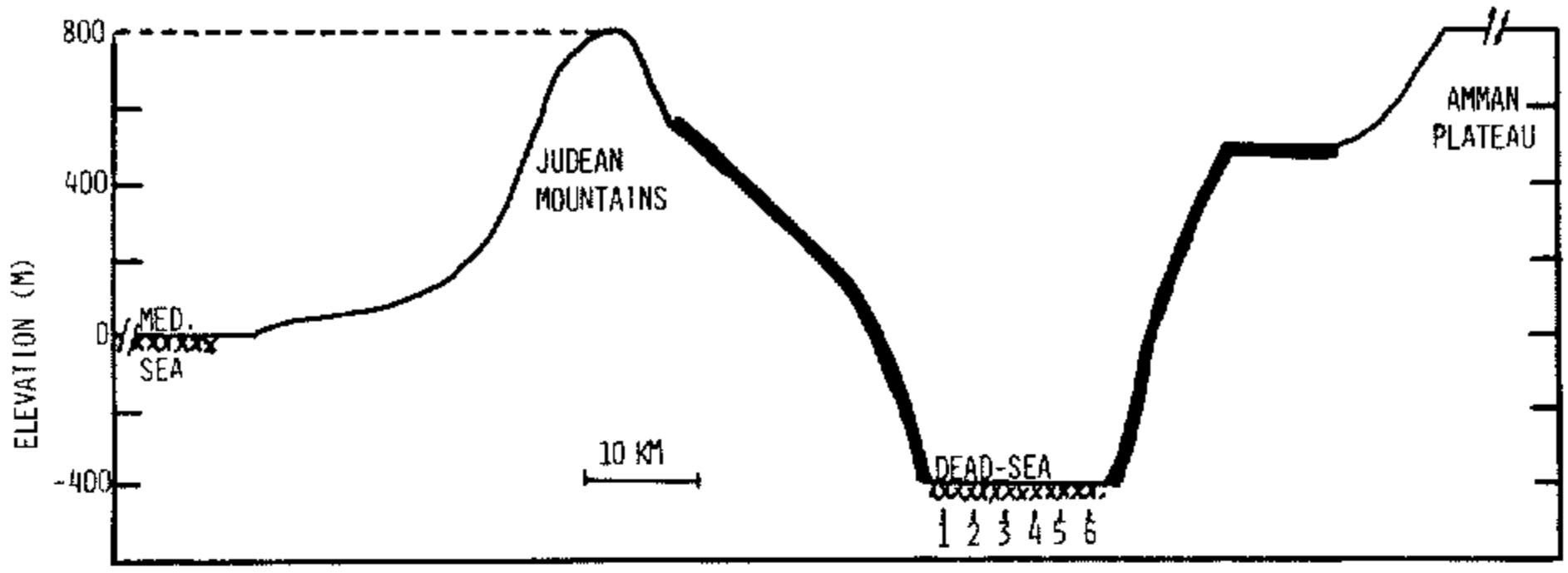

Figure 2. Schematic illustration of the terrain feature used for the 2D simulations. The darker line indicates the fine grid resolution section.

provides only a general description of patterns over the lake area. However, it illustrates deviations from the two-dimensional symmetry assumed in the 2D version. A three-dimensional simulation with the same resolution as in 2D, however, was not possible due to computer limitations. Model lateral and top boundary conditions and physical constants are the same as given in Mahrer and Pielke (1977).

With regard to boundary conditions, they consist of a zero gradient at the lateral boundaries for all predicted variables. At the surface ($z^* = 0$) the three components of the wind are required to be zero. At the model material surface top, the horizontal components of the wind are the initial geostrophic flow while the vertical component is used to move the material surface. The potential temperature at the material surface is constant, while the pressure there is computed by considering the deviation of temperature due to changes of temperature on the isentropic material surface height from the assumed initial temperature lapse at that level.

It should be stated that because of the steepness of the terrain, the use of a coordinate transformed system of equations which is valid for relatively small slopes and the use of a hydrostatic equation to represent the pressure distribution are likely to introduce some inaccuracies in the current simulations (see Pielke and Martin (1981) and Wippermann (1981)). Generally, due to the limitations imposed by the current state of the art of numerical mesoscale modelling (some of them will be discussed in the results section), we expect the results in the present study to be of a preliminary character. Nevertheless, it is worth noting that verification analyses of this model (e.g. Mahrer and Pielke (1976), Mahrer and Segal (1979), Mizzi (1982)) have indicated a reasonable model prediction skill for observed meteorological fields which are forced by irregular terrain.

4. Results

All the presented Dead Sea simulations commenced at 2000 (all times LST) following a model dynamic initialization. The summer case has been emphasized in the presentation of the results because it reflects the most persistent meteorological condition over the region. The topographic representation in the 2D figures reflects the computational terrain steepness.

(*a*) *Summer day*

During the summer (about mid-June to mid-September) the synoptic situation over the south-eastern portion of the Mediterranean region is highly persistent. It consists of a surface layer trough (Fig. 3(a)) extending from the Asiatic monsoon pressure depression, leading to a westerly flow in the lower atmosphere. In the upper layers, a subtropical anticyclone over north Africa ridges over the region resulting in clear skies.

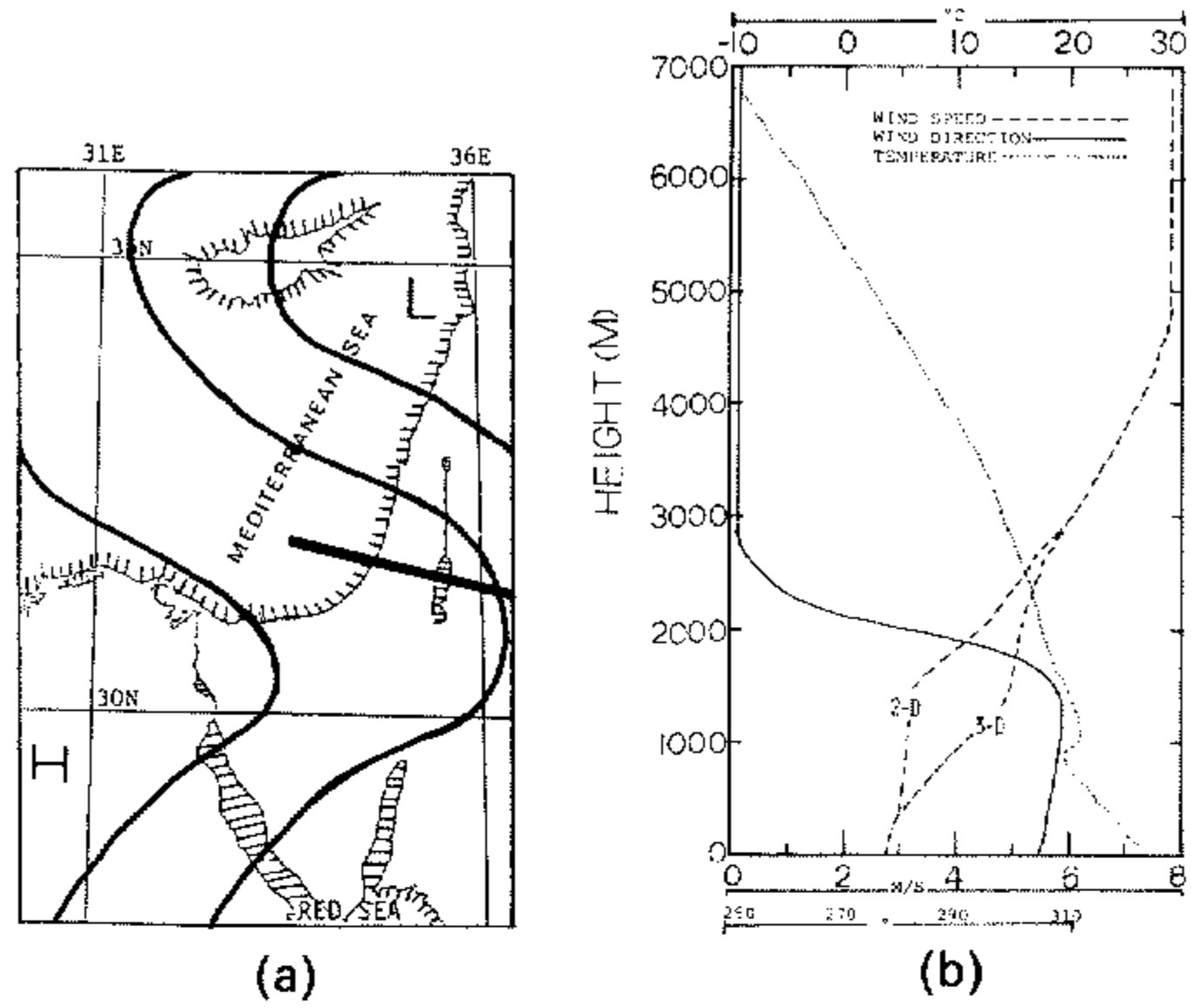

Figure 3. (a) Schematic illustration of the surface pressure system for summer day (based on Jaffe 1976). (b) Initial conditions for the summer day simulation.

Initial conditions for the summer day simulation (Fig. 3(b)) are based on Shaia's (1962) August averaged data at Be'er Ya'aqov (indicated by B on Fig. 1), including some modifications for the temperature profile as implied by the significant level data.

During summer, the penetration of the Mediterranean sea breeze (SB) circulation to the JRV during the afternoon hours is an external mesoscale process, which distorts the local circulations around the Dead Sea. However, the induced mesoscale flows in the Dead Sea area, while interacting with the synoptic Mediterranean SB flow, results in a typical daily cycle of the surface meteorological variables during the summer months as shown and discussed in the observational studies cited in section 2.

Since no major change in the Dead Sea size is expected from the channel project, the major cause of climatic change is expected to be alteration of the lake surface water temperatures. In order to investigate possible climatic modifications, two 2D simulations have been performed with the following lake surface temperatures: (1) $T_s = 33\,^{\circ}\mathrm{C}$, which is assumed to be the current August averaged lake water temperature (based on data from Ashbel (1939) and Neev and Emery (1967)); (2) $T_s = 28{\cdot}5\,^{\circ}\mathrm{C}$, which is the same as the August averaged Mediterranean Sea water temperature, representing a 'cool lake' case. (It should be noted, however, that no assessment of the final lake water temperature due to flooding with Mediterranean water was available; the assumed temperature should be regarded as an extreme choice.) 3D simulation results are also given, in order to evaluate typical climatic features over a larger-scale region, as well as to include some measure of the north–south asymmetries in the LMC.

(i) *2D simulation* ($T_s = 33\,^{\circ}\mathrm{C}$). Flow patterns at several selected times are given in Fig. 4. Towards the end of the night (0500), the coupling of the dynamically intensified flow in the lee of the mountains, due to the development of a standing wave as air flows over them and the nocturnal drainage, enhance the surface flow along the western slopes of JRV. Along the eastern slope, opposition in the directions of the synoptic and the thermal drainage flows results in some reduction of the downslope flow. Recirculation aloft over the western slopes is enhanced because of the reduction in speeds at those levels due to the standing wave. Generally, the establishment of the LMC (1100) is predicted to be

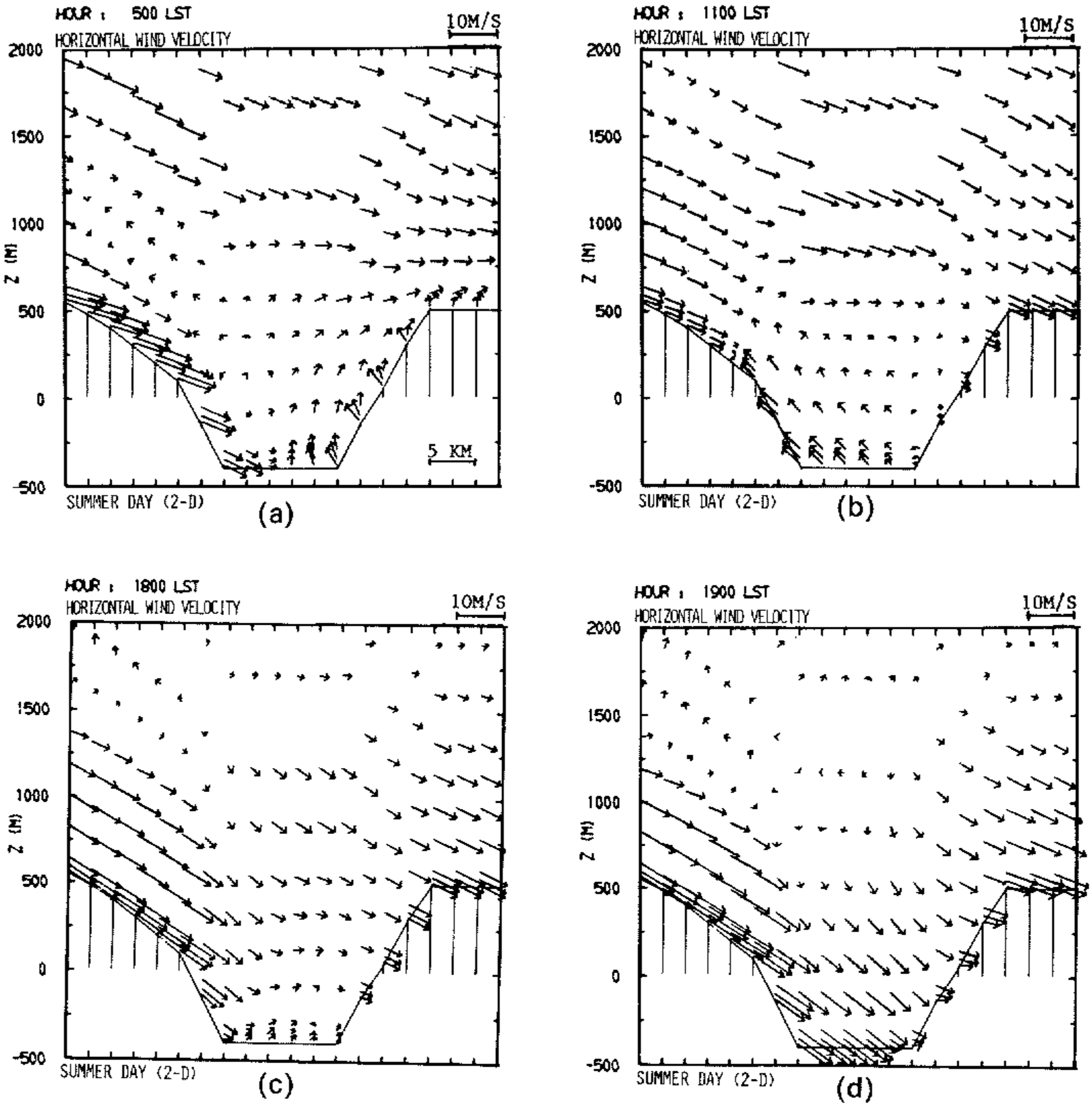

Figure 4. Horizontal wind velocities at four selected hours, along the vertical cross-section portion of the Dead Sea area (an upward vector component indicates southerly flow; a rightward component indicates westerly flow; wind speed is indicated by the scale), summer day.

asymmetrical across the lake. This asymmetric pattern is attributed to the thermally induced flows along the western slopes of the Judean mountains which, with the Mediterranean SB and the synoptic flow, causes a substantial eastward shift of the LMC along the western shore and a degeneration of the eastern LMC. The penetration of the Mediterranean SB over the lake toward evening is abrupt. Before 1800, relatively stationary flow is predicted while the Mediterranean SB penetration is delayed due to the LMC-induced counter-pressure-gradient which is directed up the western slope of the Judean mountains. At 1900, however, a rapid penetration of the Mediterranean SB is predicted over the lake. This abrupt movement is emphasized due to reduced surface roughness over the water. The return circulation associated with the Mediterranean SB is well pronounced over the western slopes.

The model-predicted daily wind speed at the western shore of the lake, as compared with observed data (from Bitan (1977) p. 298), is given in Fig. 5(a). (In this figure, and also

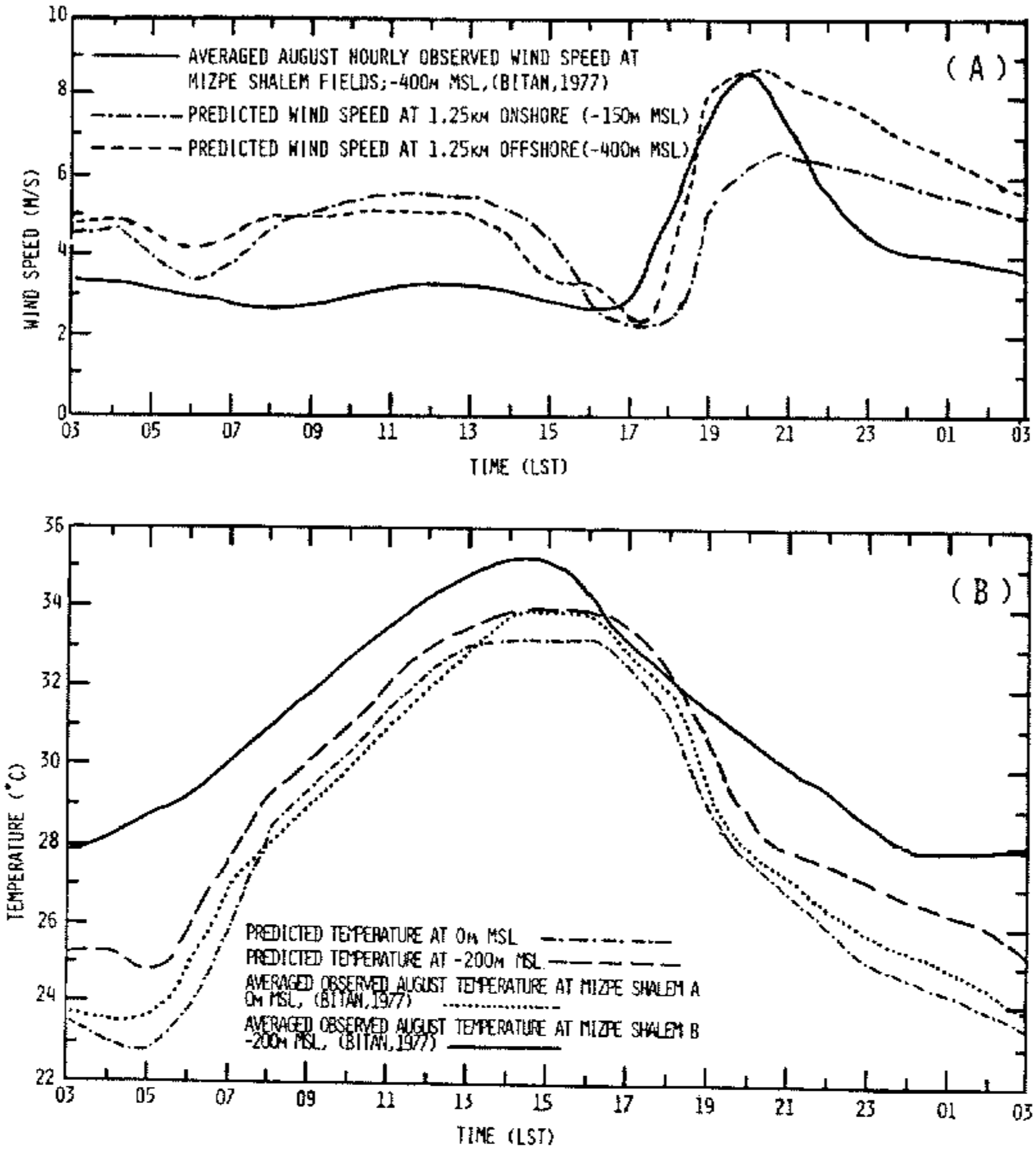

Figure 5. (a) Daily observed and predicted hourly averaged surface wind speeds along the western shore of the Dead Sea, summer day. (b) Daily observed and predicted temperature at meteorological shelter level on the western shore of the Dead Sea, summer day.

Fig. 5(b), predicted values are illustrated beginning with 0300, 7 h after the beginning of the simulation, in order to avoid possible misrepresentations associated with the initial conditions.) The Mizpe Shalem Fields wind speed is compared with hourly predictions at grid points located 1·25 km offshore and 1·25 km onshore (the station is located on the Dead Sea shoreline, F in Fig. 1). The general pattern of the predicted wind speed, including the abrupt penetration of the Mediterranean SB onto the Dead Sea towards evening, is in agreement with the observed pattern. Reasons for the differences between predicted and observed values are discussed in (*a*, iii) below.

The diurnal variations of model-predicted temperature at a height of 2 m for distances of 1·25 km (200 m below MSL) and 3·75 km (at MSL) onshore show an elevation effect on temperature (Fig. 5(b)). Daily maximum temperatures occur in the afternoon, due both to solar insolation and adiabatic compression, as the Mediterranean SB descends along the western JRV. Observed and predicted daily cycles of temperature are in good agreement except during the nocturnal period at the lower site, where predicted temperatures are significantly lower than observed, apparently due to the highly irregular local terrain, which is unresolved by the model grid.

(ii) *2D simulation* ($T_s = 28{\cdot}5$ °C). The simulation of the previous section was again carried out, but with lake surface water temperature reduced to 28·5 °C. Selected changes (given

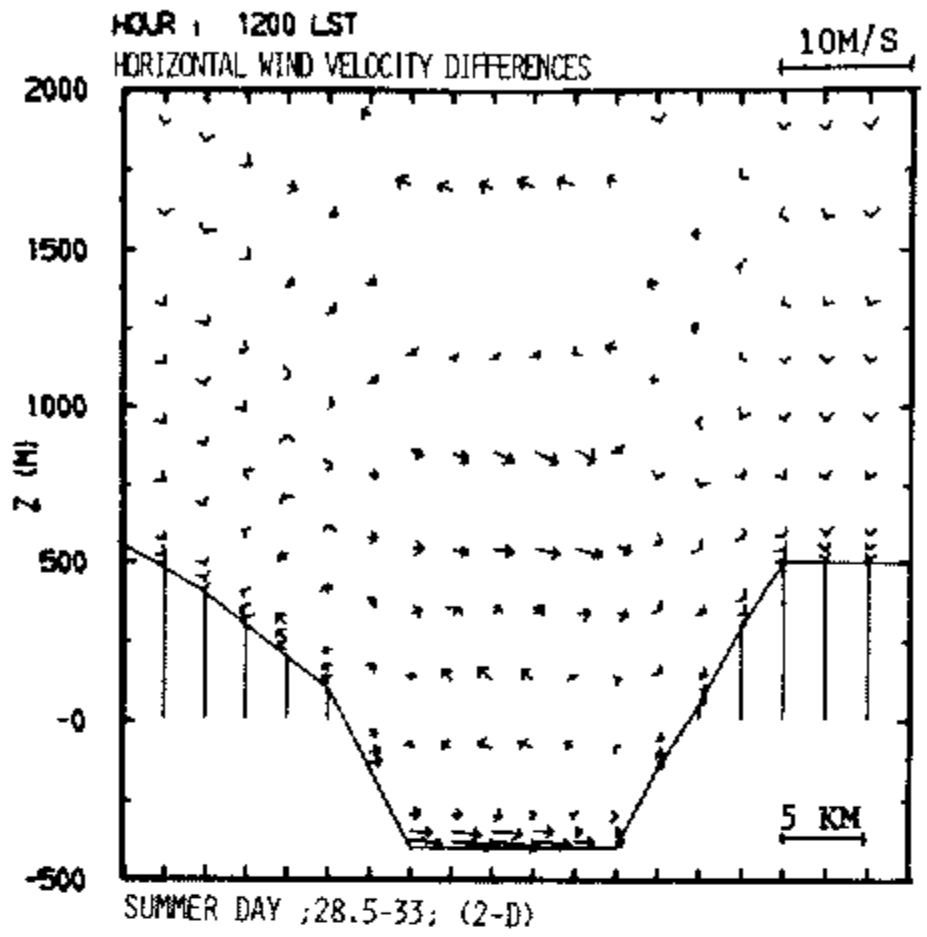

(a)

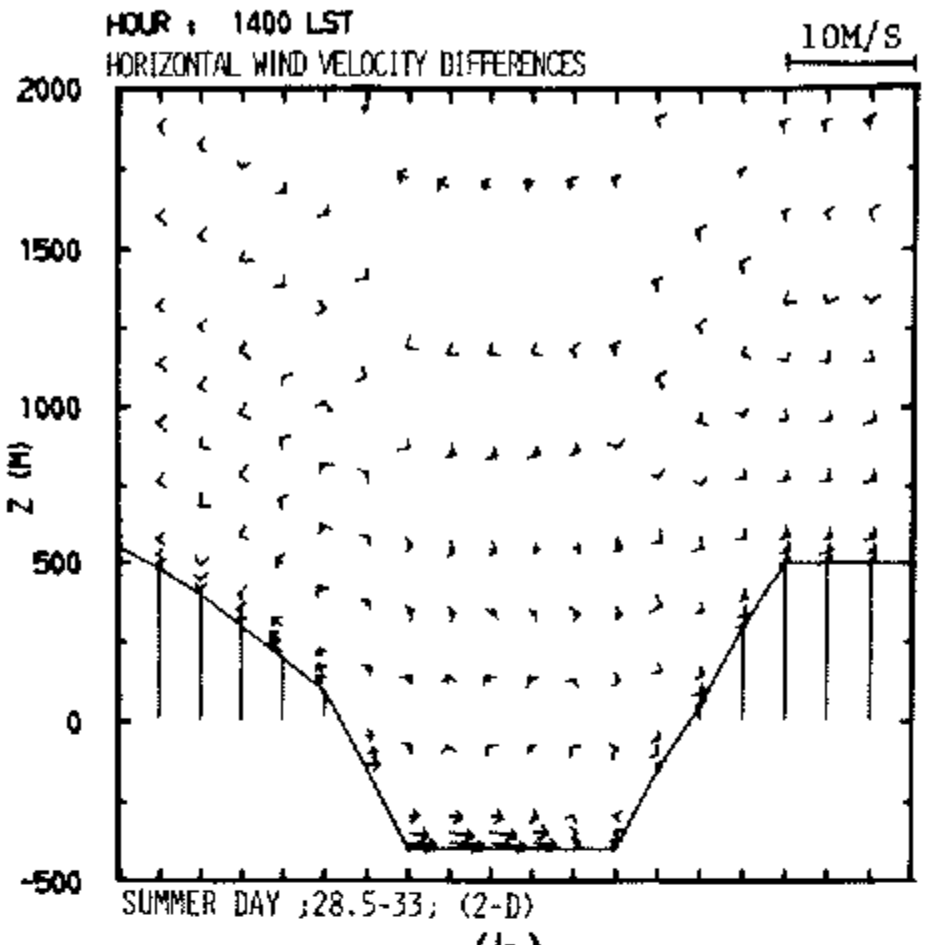

(b)

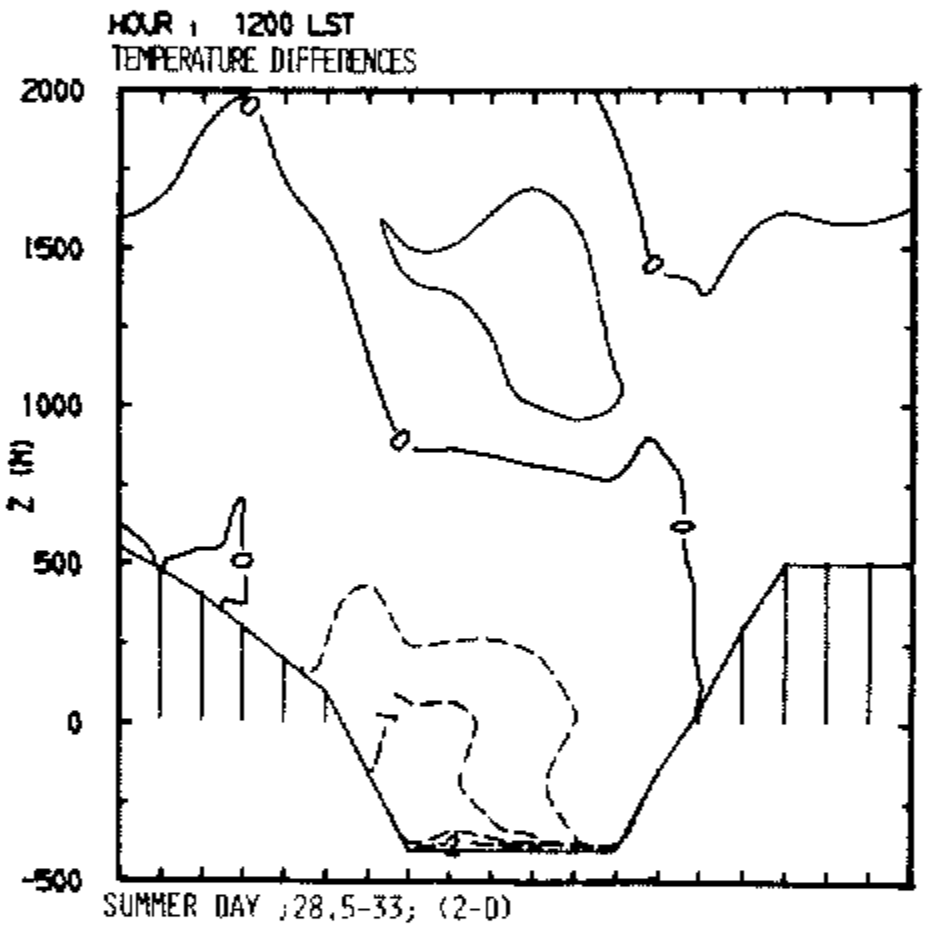

(c)

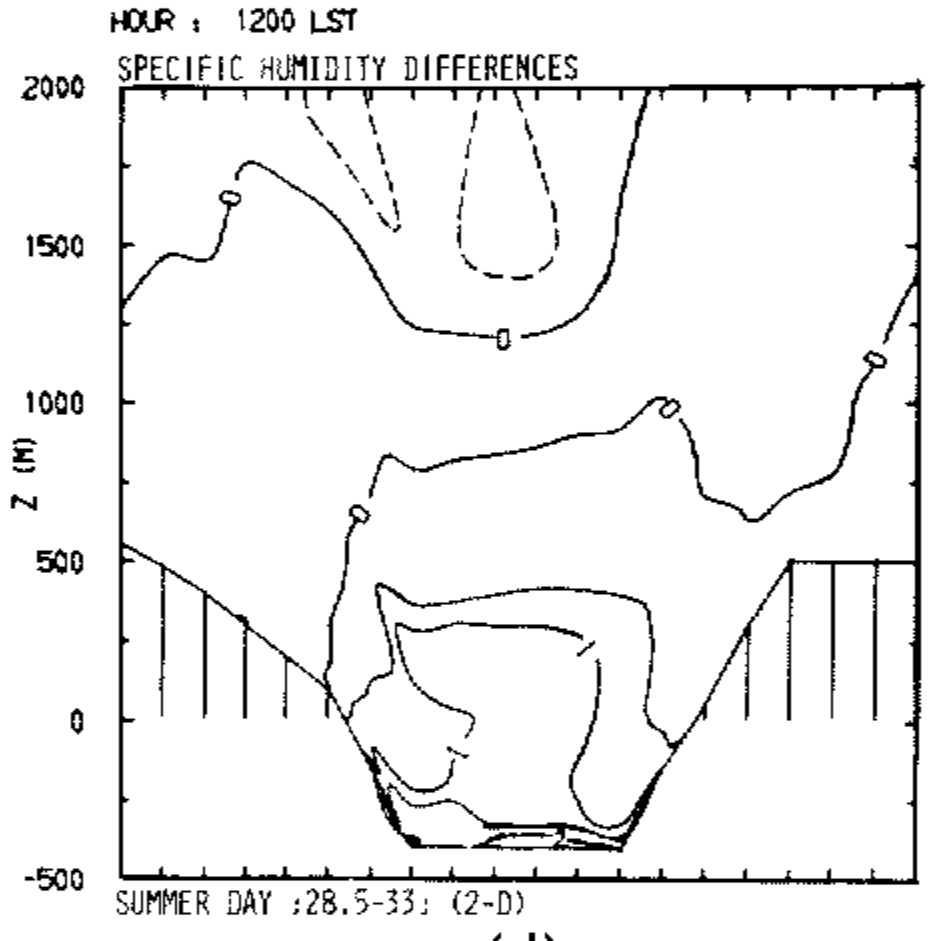

(d)

Figure 6. Selected patterns of differences in meteorological fields which result when the lake water temperature is changed from 33 °C to 28·5 °C. The fields presented refer to ($\Psi_{28\cdot5} - \Psi_{33}$) where Ψ relates to : (a) and (b) horizontal wind velocities; (c) temperature (°C); and (d) specific humidity ($g\,kg^{-1}$) (dashed contours indicate negative values), summer day.

as differences between the 28·5 and 33 °C fields) for wind, temperature and specific humidity are shown in Fig. 6. Generally, changes in the patterns are restricted to the lake itself, diminishing sharply even a short distance onshore. Concerning the wind velocity, it is found that the easterly wind component has been reduced over the lake and somewhat over the lower eastern slopes as illustrated at 1200 and 1400. (A physical explanation for this change, in the absence of the complicating effects of external mesoscale and synoptic flows, will be given in sub-section (*b*).) Along the lower western slopes, which are affected by a more intense LMC than the eastern shore in the control experiment, the temperature reduction is more pronounced (Fig. 6(c)).

The major forcing factors governing the spatial distribution of moisture over the lake are the rate of evaporation, advection, and vertical diffusion. Additionally, it should be noted that, in our case, moisture originating over the Mediterranean Sea is advected to the Dead Sea region. Figure 6(d) presents a typical pattern for noon. It is clear that the stabilization of the atmosphere over the cold lake, which results in poor vertical diffusion,

leads to an accumulation of moisture in the lower atmosphere over the cold lake, even though the warm lake evaporation rate is larger (see Table 2). On the other hand, because of the intense vertical mixing over the warm lake, moisture penetrates to higher layers where it is advected out of the domain by the strong westerly winds aloft. In the cold lake case, the upper layer is deficient in moisture (due to the lower evaporation rate, and eastward advection not being replenished by turbulent upward moisture flux from below), whereas in the intermediate layers differences are negligible. In the evening, in contrast, as the lake is affected by a strong low-level flow in the lower atmosphere, due to the penetration of the Mediterranean SB, advection becomes dominant so that deficiencies in moisture over the lower atmosphere of the cold lake are predicted (not shown).

(iii) *3D summer simulation.* Considering the large extent of the region which influences the Dead Sea meteorological patterns (mostly during daylight hours), the imposition of an infinite mountain ridge, as assumed in the 2D simulation, may somewhat affect the realism of the solutions. Additionally, one should notice that there is also some deviation from two dimensionality with regard to the longitudinal orientation of the Mediterranean shore and the Dead Sea. Due to this type of departure from the idealized terrain in the greater Dead Sea region, the performance of a 3D test simulation using the same initial vertical profile of the horizontal wind as in the 2D case, indicated some reduction in the wind speed along the eastern side of the Judean mountains. This difference between the simulations is attributed mostly to the more vigorous forced mountain wave flow induced by the rigid infinite topography of the 2D case. In order to match the flow patterns of both cases, the initial wind profile of the 3D simulation was modified by using the averaged August wind speeds, and not the speed of the August averaged wind velocity (as in the 2D case), which is somewhat lower. It should be pointed out that the differences between these two profiles (with a maximum difference of 2 $m\,s^{-1}$), indicate that a more refined resolution of the summer flow patterns should consider the categorization into different representative vertical profiles of the horizontal wind. The purpose of the 3D simulation is mostly to provide some insight to possible asymmetries in the meteorological patterns.

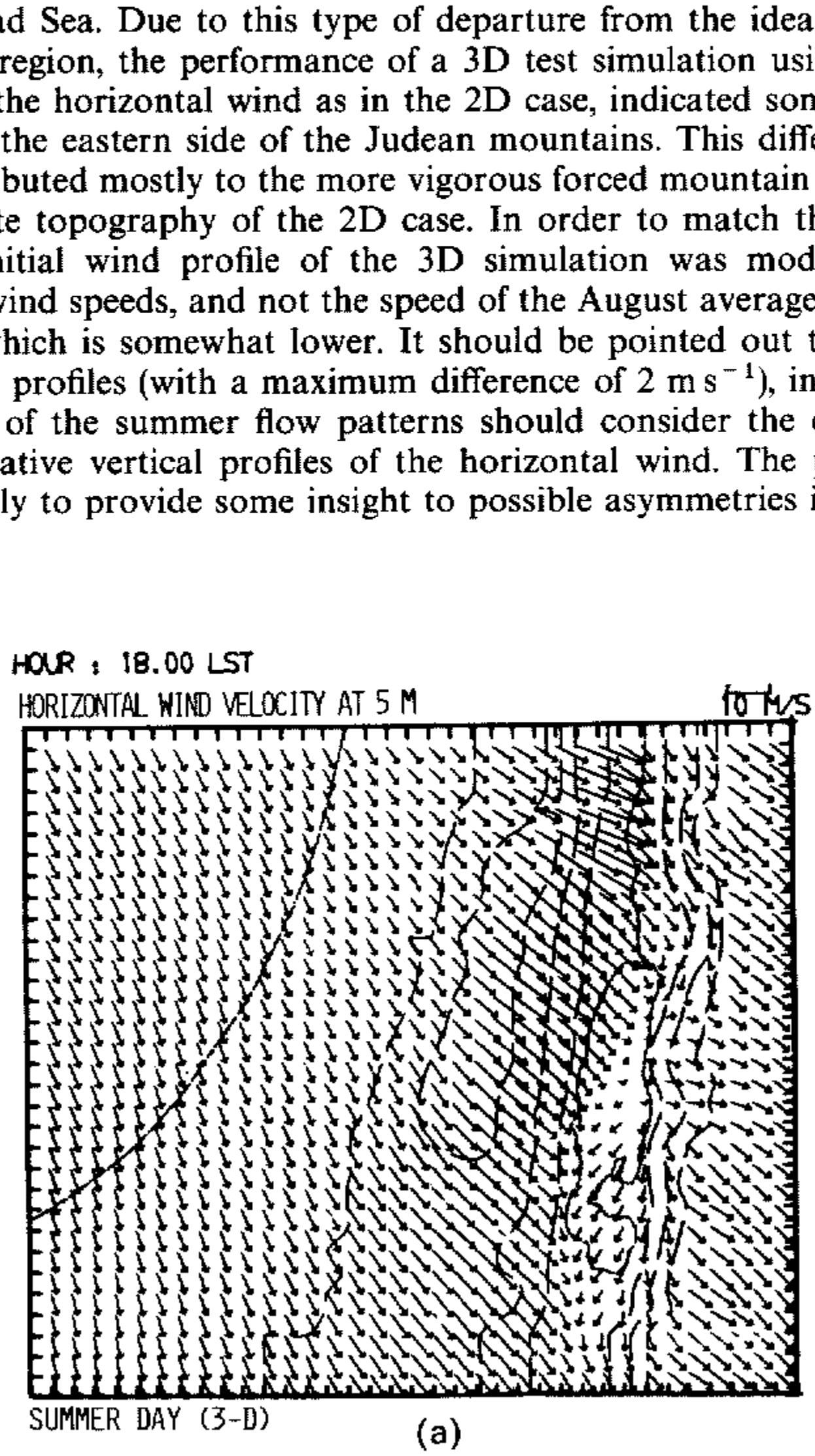

Figure 7(a). Simulated horizontal wind field at 1800 (LST).

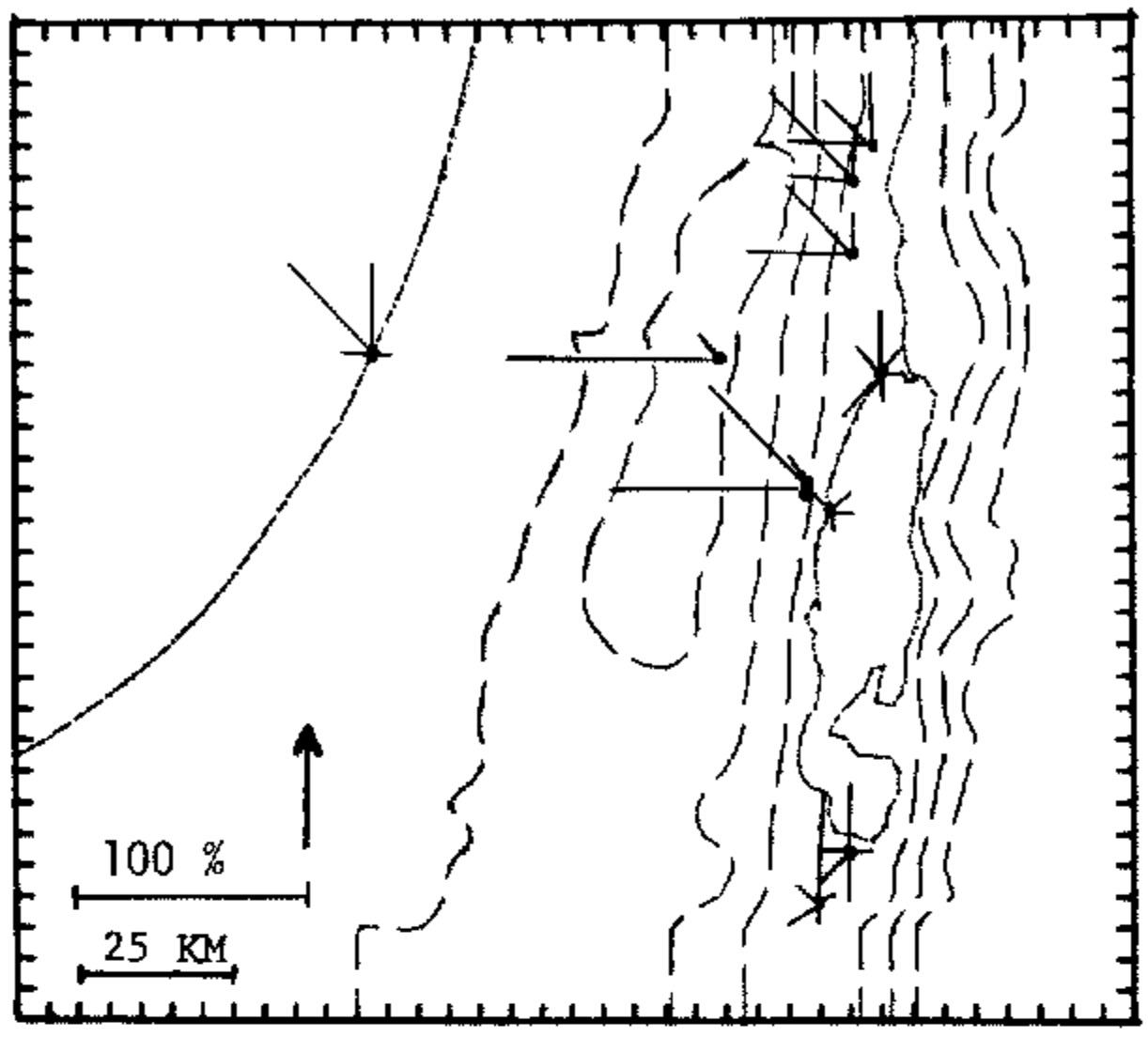

(b)

Figure 7(b). August wind roses for several sites, at 1800. The scale for 100% frequency is shown (from Bitan 1974, 1977).

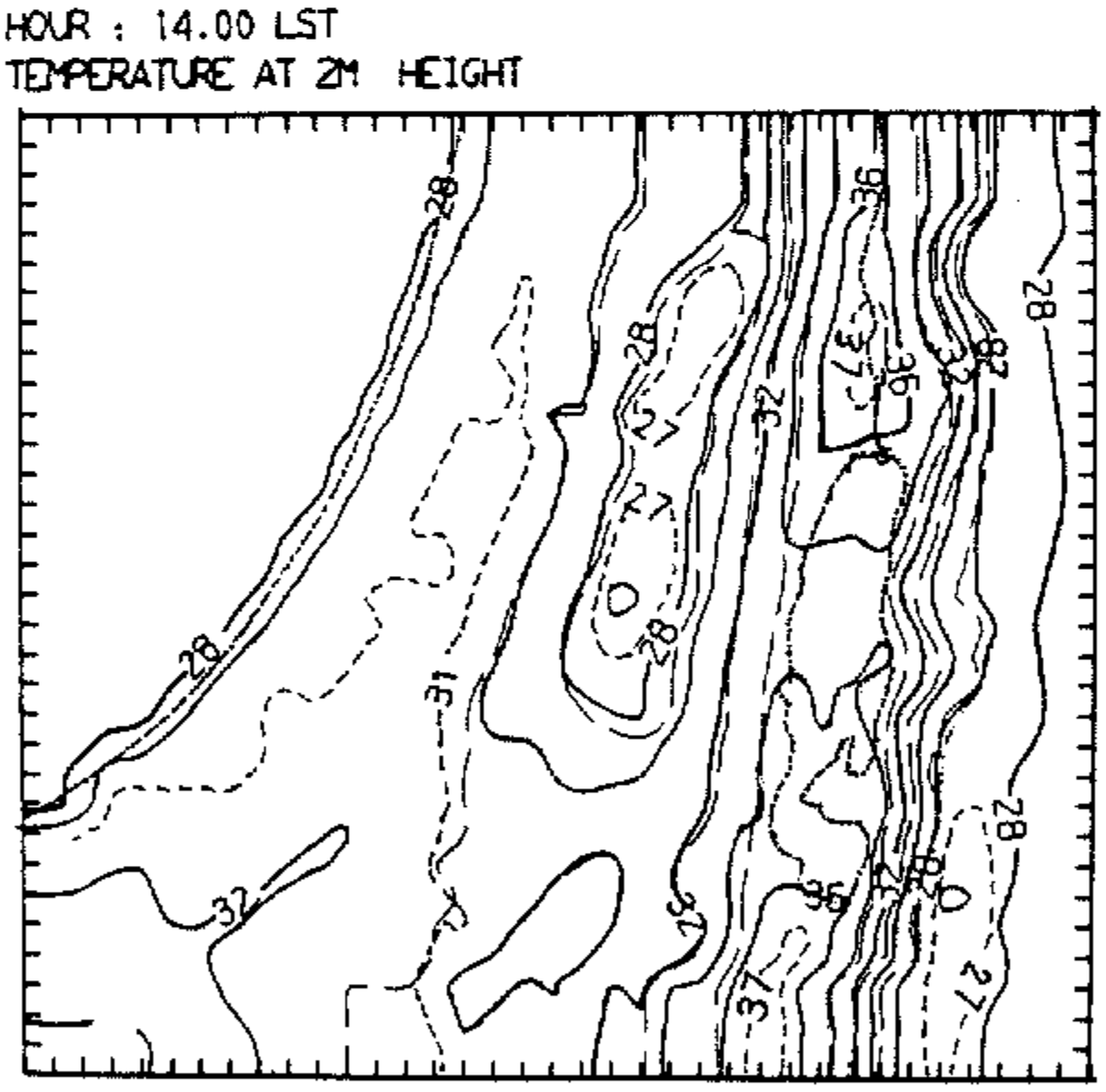

(c)

Figure 7(c). Simulated 2 m height temperature field at 1400, 3D simulation, summer day.

Figure 7(a) illustrates the flow at 5 m at 1800. The penetration of the Mediterranean SB towards the northern section of the JRV, which is closer to the Mediterranean shore, occurs earlier than in the remote southern section. This pattern, which is supported by the observational studies mentioned in section 2, cannot be resolved, of course, by a 2D simulation. Additionally, the apparent error in wind direction predicted using the 2D version over the Dead Sea during the penetration of Mediterranean SB (slight southwesterly as indicated in Fig. 4(c)), was eliminated in the 3D prediction, where the observed northeasterly flow, based on several available offshore wind measurements, was accurately

predicted. Figure 7(b) presents observed wind roses for several sites, which indicate reasonable predictions for the flow directions. The model-predicted temperature field at 2 m by 1400 is given in Fig. 7(c). It illustrates the well-known observed temperature pattern at noon during summer (e.g. *Atlas of Israel* 1970). In the west–east direction, regions with local temperature maxima are located along the inner coastal area and the JRV. The correlation of temperature with topography is pronounced, as isotherms tend to be oriented parallel to the height contours. In the near vicinity of the lake, some reduction in temperature due to the local breeze is predicted. The predicted temperatures resemble August averaged observed temperatures throughout the domain (Segal *et al.* 1982b),

(*b*) *Analysis of the effect of mountain slope steepness and lake water temperature on the LMC*

In order to estimate the effects of the steepness of the mountain slope and lake water temperature on the LMC, the circulation theorem has been applied along a cross-section perpendicular to the slopes, illustrated in Fig. 8. Using a terrain-following coordinate system, with the equation and symbols given in Mahrer and Pielke (1977, p. 100), the change in circulation with time along the illustrated path is given by

$$\partial\left(\oint u\,dl\right)\Big/\partial t \simeq \int_s \{-(\partial\theta/\partial z^*)(\partial\pi/\partial x) + (\partial\theta/\partial x)(\partial\pi/\partial z^*) + (\partial F/\partial z^*)\}\,ds \qquad (1)$$

where

u = upslope wind component
π = Exner pressure function = $c_p\,T/\theta$
θ = potential temperature
z^* is the vertical coordinate = $H(z - z_G)/(H - z_G)$,

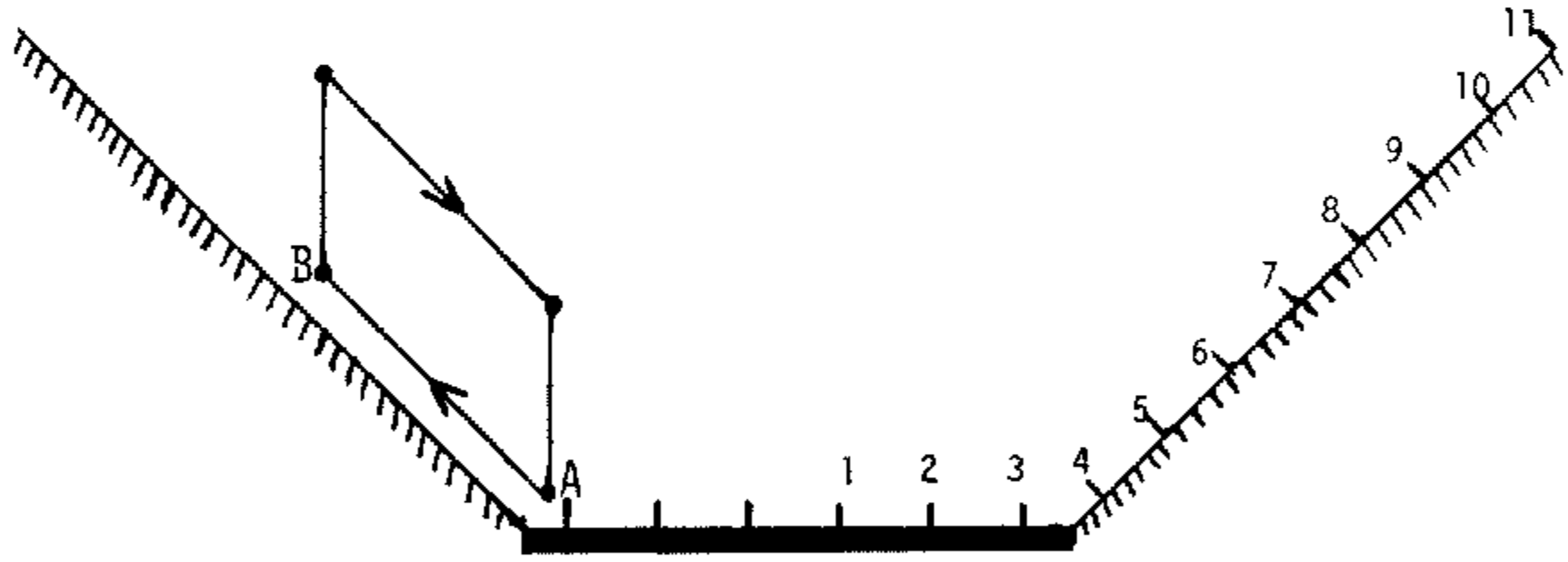

Figure 8. Schematic illustration of the path chosen for LMC evaluation.

with H the initial model top height, z_G the topography elevation, S the area of the vertical cross-section, and $\partial F/\partial z^*$ consists of the contributions from vertical fluxes of momentum. (Following Anthes (1978), advection terms were assumed to be small compared with the solenoid term and they were not considered in the analysis. Also, the Coriolis term was not considered to be of importance for the ongoing analysis.)

Assuming an initial equilibrium situation, with no flow, at sunrise and using the relation

$$\partial\bar{\pi}/\partial x \simeq (\partial\bar{\pi}/\partial z^*)(\partial z_G/\partial x), \qquad (2)$$

where overbar indicates an initial value, we have at $t = 0$

$$\partial\left(\oint \bar{u}\,dl\right)\Big/\partial t = \int_s [\{-(\partial\bar{\theta}/dz^*)(\partial z_G/\partial x) + \partial\bar{\theta}/\partial x\}(\partial\bar{\pi}/\partial z^*)]\,ds = 0. \qquad (3)$$

Following sunrise, pressure and potential temperature are perturbed, resulting in commencement of LMC with its temporal intensity variation given by

$$\frac{\partial}{\partial t}\oint u'\,dl = \int_s \left\{ -\left(\frac{\partial \bar{\theta}}{\partial z^*} + \frac{\partial \theta'}{\partial z^*}\right)\frac{\partial z_G}{\partial x} + \left(\frac{\partial \bar{\theta}}{\partial x} + \frac{\partial \theta'}{\partial x}\right)\frac{\partial}{\partial z^*}(\bar{\pi} + \pi') + \frac{\partial F}{\partial z^*}\right\} ds \tag{4}$$

where prime indicates a deviation from the initial field. Since $|\partial\bar{\pi}/\partial z^*| \gg \partial\pi'/\partial z^*$, using Eq. (3) we get

$$\partial\left(\oint u'\,dl\right)\Big/\partial t \simeq \int_s [-\{(\partial\theta'/\partial z^*)(\partial z_G/\partial x) + \partial\theta'/\partial x\}(\partial\bar{\pi}/\partial z^*) + \partial F/\partial z^*]\,ds. \tag{5}$$

Choosing the top path of Fig. 8 to be the zero wind speed height (following the studies of, for example, Johnson and O'Brien (1973), Anthes (1978), Mizzi (1982), this is also the height of the planetary boundary layer) associated with the LMC, and neglecting the small contribution of the lateral section of the path to the circulation (which is due to the vertical velocities), then Eq. (5) becomes

$$\partial\left(\int u'\,dl\right)\Big/\partial t \simeq \int_s [\{-(\partial\theta'/\partial z^*)(\partial z_G/\partial x) + \partial\theta'/\partial x\}(\partial\bar{\pi}/\partial z^*)]\,ds + \int F\,dl, \tag{6}$$

the line integrals running from A to B. Since the following inequalities hold along the western sloping shore of a lake,

$$\partial\bar{\pi}/\partial z^* < 0; \qquad \partial\theta'/\partial x < 0; \qquad \partial z_G/\partial x < 0 \tag{7}$$

therefore, when $\partial\theta'/\partial z^*$ tends to become positive at the lake vicinity as the lake atmosphere cools (i.e. as lake water temperature reduces), the first term in the first right-hand integral of Eq. (6) reduces the circulation. On the other hand, the second term in that integral increases the circulation. Hence, in cases where $\partial\theta'/\partial z^* > 0$, if

$$|\partial z_G/\partial x| > \left|\int_s \frac{\partial\theta'}{\partial x}\,ds\right| \Big/ \left|\int_s \frac{\partial\theta'}{\partial z^*}\,ds\right| \simeq Z_i/L \tag{8}$$

then the areal integral of (6) will have a negative contribution to the circulation. The right-hand side of (8) can be approximated as the ratio of the scale of the planetary boundary layer height, Z_i, and the horizontal scale of the LMC, L. Assuming no major changes in F and in the size of the circulation, S, as the slope steepness changes or as lake water cools, (8) provides an estimate as to when the terrain slope is steep enough to retard the LMC intensity. Equation (8) suggests that:

(i) The tendency toward retardation of the LMC increases as the slope of the mountain steepens.

(ii) For a given mountain slope, thermal stabilization of the surface atmosphere as a result of cooling the water surface may tend to weaken the LMC for a small offshore section. In this section, a reduction of Z_i is caused as the lake cools due to the decrease in the thermally generated turbulence (Z_i is not affected there by thermally induced upward velocities as the LMC is well developed), based on (8) in such a situation the LMC will maintain its intensity in that section only if the horizontal thermal gradient increases appropriately.

(c) *Illustrations of the slope–lake temperature effect on the LMC*

Several simulations with representative combinations of moderate mountain slopes ($\alpha = \partial z_G/\partial x$) and lake surface water temperature, T, have been carried out, using a horizontal grid interval of 3 km and 6 grid points for the representation for the lake area as

TABLE 1. THE UPSLOPE WIND SPEED ($cm\,s^{-1}$) AT 5 m HEIGHT ASSOCIATED WITH THE LMC FOR VARIOUS COMBINATIONS OF TERRAIN SLOPES, α, AND LAKE WATER TEMPERATURE, AND FOR THE NO-LAKE CASES. FOR GRID POINTS SEE FIG. 8.

		Grid point										
		Lake (half size)			Along the slope							
T °C	α	1	2	3	4	5	6	7	8	9	10	11
18·5	5/300	31	139	272	352	398	423	414	399	398	396	394
18·5	10/300	24	112	219	295	373	442	472	474	468	467	472
18·5	20/300	39	79	132	268	408	490	537	546	549	554	557
28·5	5/300	24	143	301	376	413	433	417	401	399	397	395
28·5	10/300	22	136	277	330	382	445	472	475	468	468	472
28·5	20/300	33	128	242	322	413	491	537	548	550	556	556
No lake	5/300	85	150	205	245	245	236	254	295	334	352	363
	10/300	110	157	200	259	314	368	410	427	433	443	456
	20/300	135	195	265	368	427	464	511	534	544	544	552

shown in Fig. 8. The models have been integrated from sunrise to 1300. The upslope components of the predicted wind velocity at that hour (including also no-lake cases) for the various combinations are given in Table 1, from which the following results can be stated:

(i) For given α, the results indicate that $u_{28\cdot5} > u_{18\cdot5}$ immediately surrounding the lake (u is the upslope flow component; the subscript refers to the lake temperature). However, $u_{28\cdot5} \simeq u_{18\cdot5}$ well inland from the lake.

(ii) For $\alpha_1 > \alpha_2$ and given T, the results indicate that $u(\alpha_1) < u(\alpha_2)$ in the vicinity of the lake. However, far from the lake, where the lake breeze contribution to the thermal stabilization diminishes and the steepest slope has the more intensive upslope flows, $u(\alpha_1) > u(\alpha_2)$.

(iii) For given α and comparison of lake (l) and no lake (nl) cases, $u(nl) < u(l)$ at several grid points along the slopes (if α is small enough), while $u(nl) \simeq u(l)$ far from the lake.

These relations, although based on a limited number of simulations, support the implications suggested by Eq. (6) in the previous section. It is interesting to note that, when temperatures over the lake were forced to become lower than those obtained in the presented simulations (by a second series of simulations where the lake negative heat influxes to the atmosphere are artificially increased), relations (i) to (iii) are even more emphasized.

(*d*) *Winter day*

During winter the region is affected by the passage of mid-latitude synoptic waves. High pressure systems, as illustrated in Fig. 9(a), frequently occur, resulting in clear skies and light synoptic winds (Levi 1967). The flow patterns along the JRV in such conditions are highly dominated by the local LMC.

Initial conditions for temperature and moisture in this simulation were prescribed according to representative data from the Be'er Ya'aqov radiosonde station, (Fig. 9(b)). Towards the end of the night (0600), because of the slight synoptic flow parallel to the Dead Sea, a relatively symmetrical LMC is predicted along both slopes (Fig. 10(a)). This symmetry is reflected in the vertical velocity pattern, which shows a convergence zone in the middle of the lake (Fig. 10(b)). This pattern suggests that the LMCs due to the Dead Sea topographical effects are highly symmetrical around the centre of the lake. The LMC was indicated to be symmetric also in the morning hours. However, gradually it became asymmetrical as illustrated in Fig. 10(c) for 1500 (about two hours before sunset). At this time, a well-established closed circulation dominated the western slopes and lake, whilst

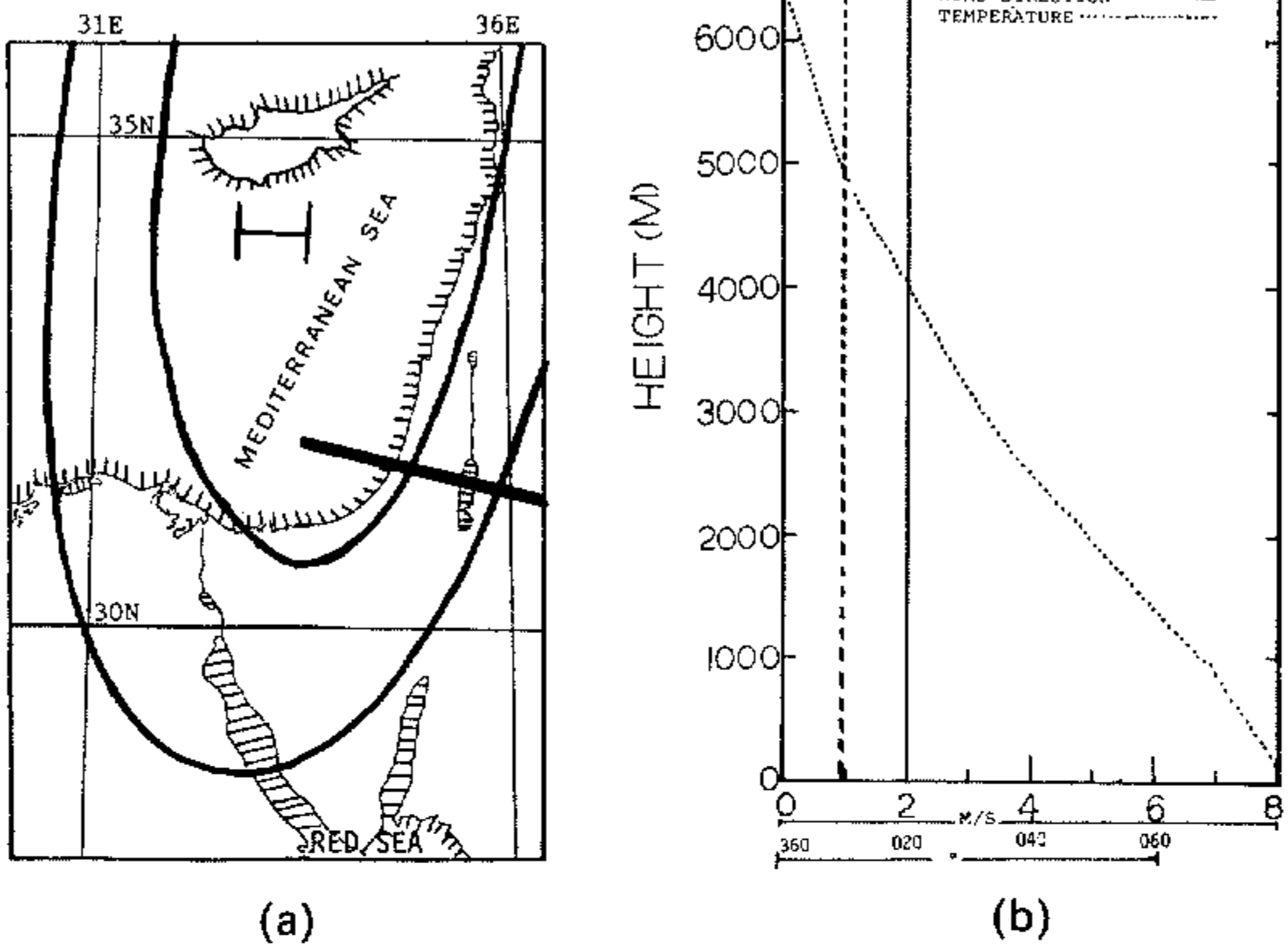

Figure 9. (a) Schematic illustration of the surface pressure system for the winter day case (based on Levi 1967). (b) Initial conditions for the winter day simulation.

the eastern circulation had almost disappeared. It is assumed that the cause of this daylight asymmetry is the combined effect of thermally induced upslope flows and the Mediterranean SB along the western side of the Judean mountain. (During the winter, the Mediterrranean SB is too weak to penetrate to the JRV, see, e.g., Ashbel 1939; Bitan 1977.) A hypothetical simulation of the winter day, where the Mediterranean Sea is eliminated and an 800 m plateau created west of the Judean mountains (as indicated by the dashed line in Fig. 2), indeed confirms this hypothesis. The result of this latter experiment is the re-establishment of two relatively symmetrical LMCs at the Dead Sea, as shown in Fig. 10(d)).

(e) *Evaporation rates over the lake*

Referring to the practical point of view of the potential channel project to carry Mediterranean water to the Dead Sea, evaporation rates from the water surface are of major importance. Assessments for the evaporation rates for the various situations were carried by using the relation

$$E = \rho u_* q_* \tag{9}$$

where ρ is air density, u_* the friction velocity and q_* the flux specific humidity. The lowering of the saturation mixing ratio due to water salinity is approximated in Eq. (9) according to Krauss (1972) p. 46. The reduction for the Dead Sea for this experiment was estimated to be 10% (rough scaling suggests that q_* will be reduced by a similar amount). Computed evaporation rates are given in Table 2. The reduction of the lake surface temperature in the summer to 28·5 °C results in a sharp decrease in evaporation rates because of the creation of a stable layer over the lake with a subsequent reduction of u_* and q_*. In the winter case, the relatively low water temperature (21 °C) reduces the saturation moisture value over the lake, compared with the modified summer case.

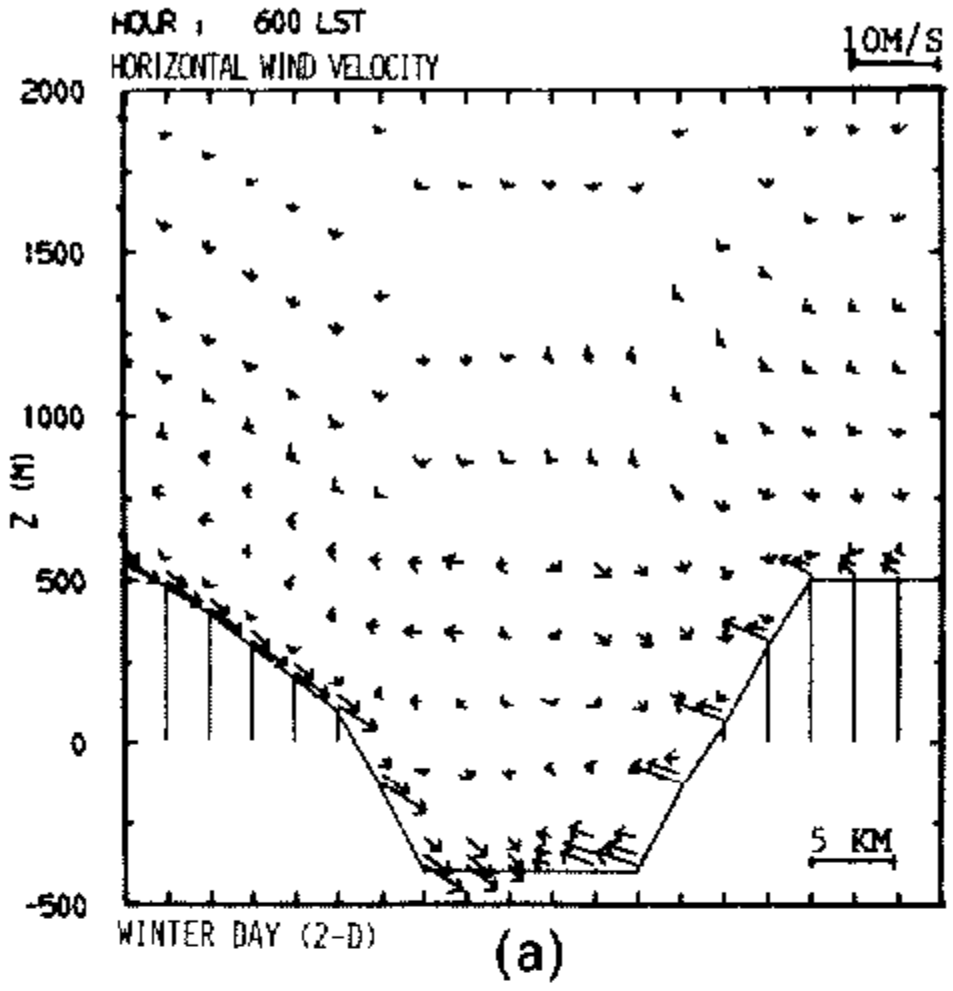

(a)

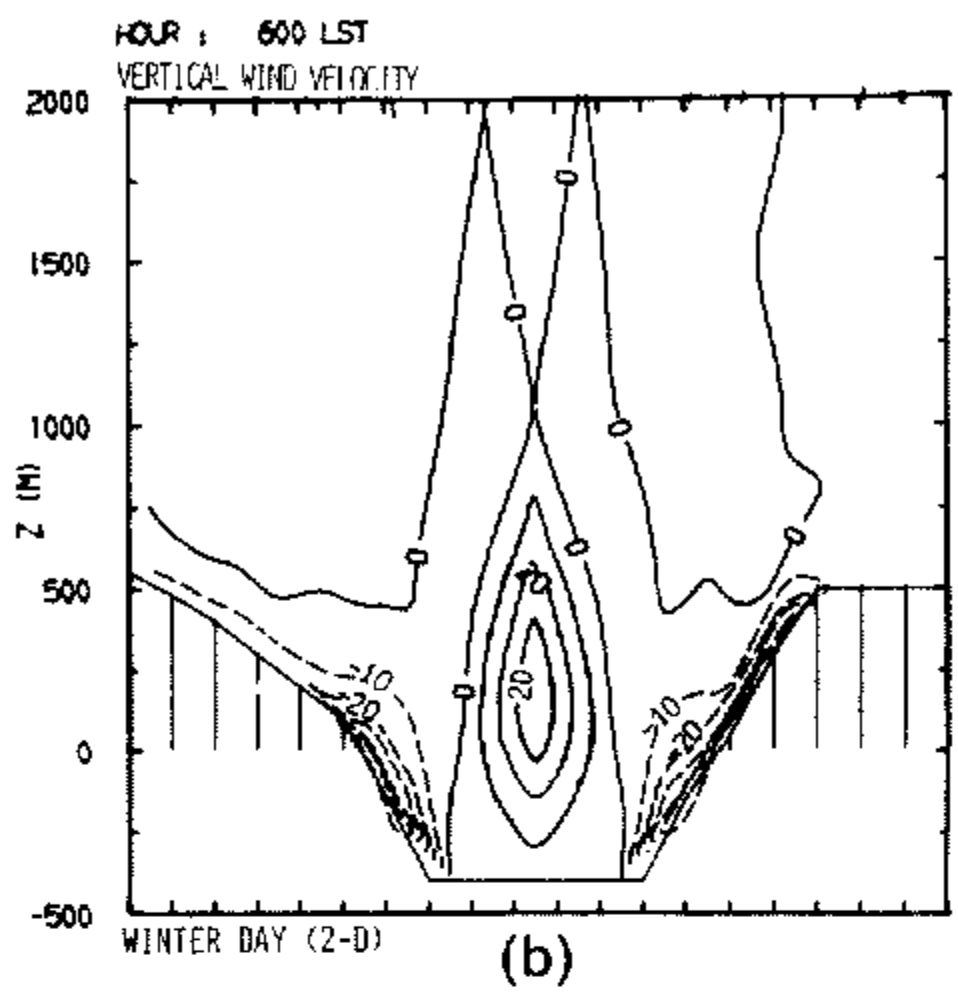

(b)

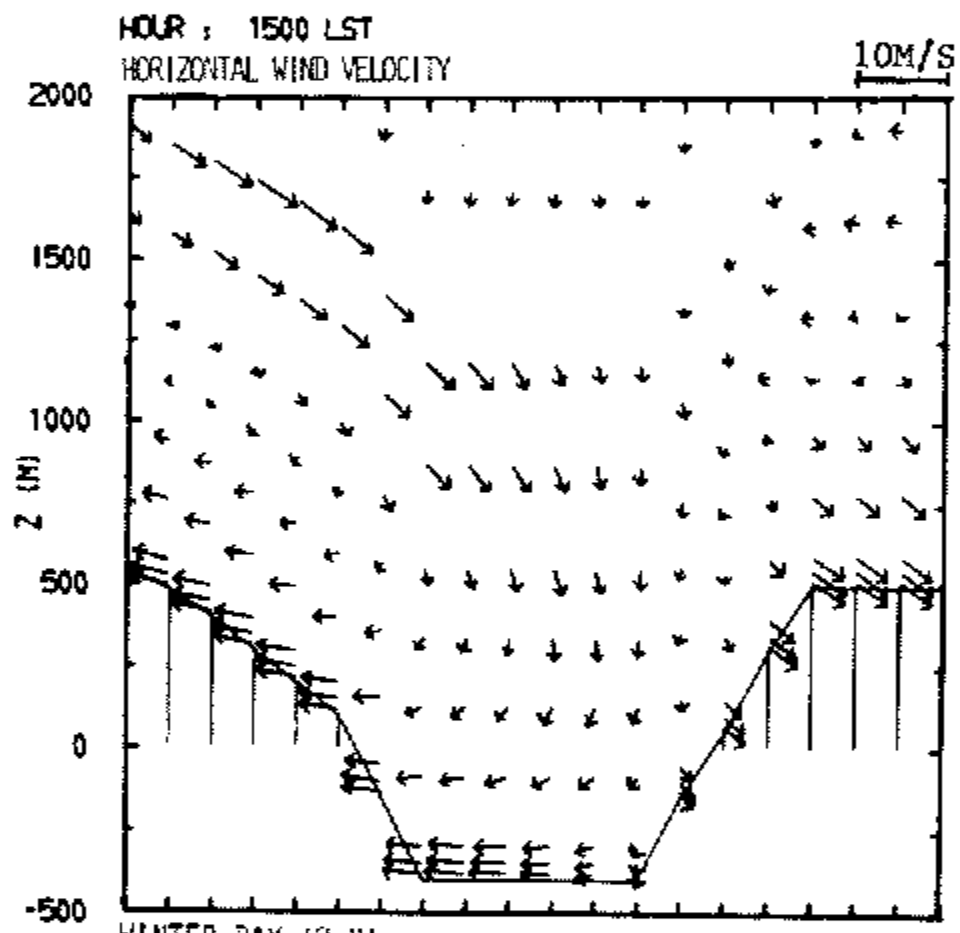

(c)

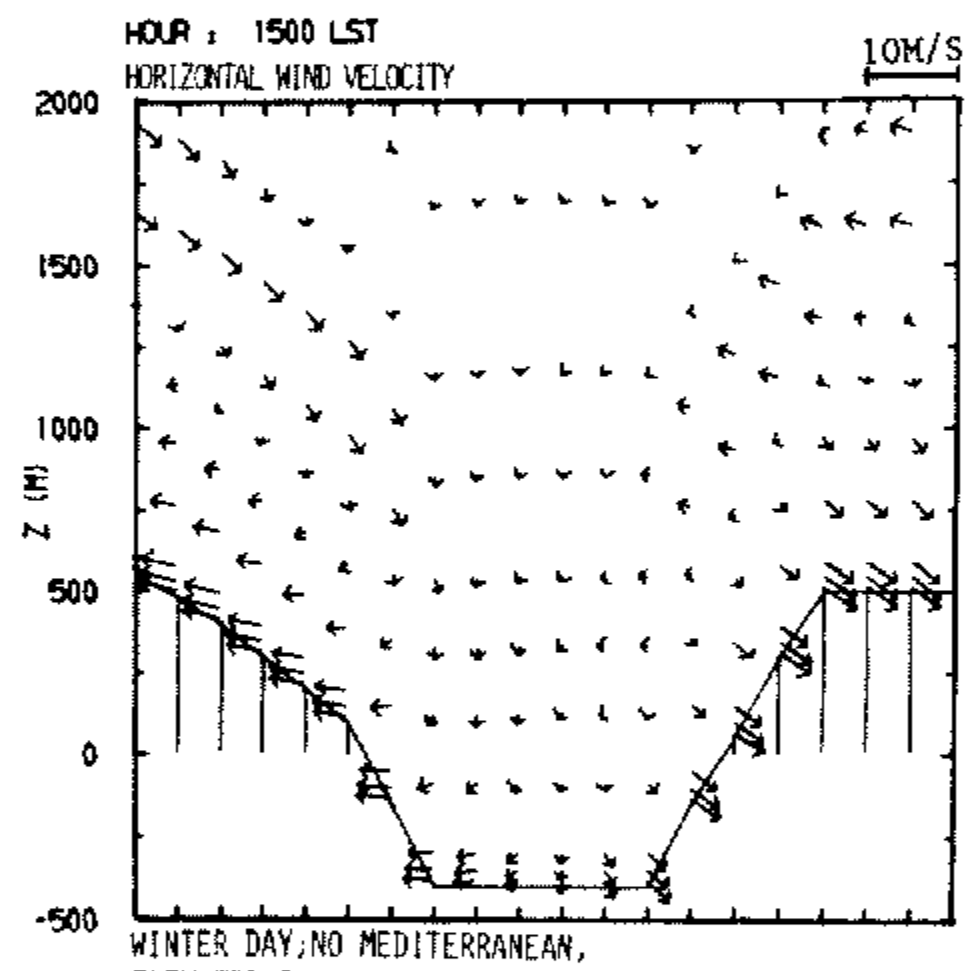

(d)

Figure 10. Winter day. (a) and (c). Horizontal wind velocities, at 0600 and 1500 (LST) respectively. (b) The vertical wind speed (cm s^{-1}) at 0600. (d) The horizontal wind velocities at 1500, where the terrain feature was modified as illustrated by the dashed line in Fig. 2.

TABLE 2. EVAPORATION RATES (mm d^{-1}) ALONG THE DEAD SEA CROSS-SECTION AT THE POINTS INDICATED IN FIG. 2.

	Grid point						
	1	2	3	4	5	6	Average
Summer day, $T_s = 33\,°C$	8·8	7·6	6·5	6·2	5·2	4·6	6·5
Summer day, $T_s = 28{\cdot}5\,°C$	3·4	2·6	1·8	1·7	1·8	1·9	2·2
Winter day	5·3	4·9	3·6	3·2	3·9	4·5	4·2

However, the winter day evaporation rates are higher because they are associated with an unstable thermal stratification within the lake atmospheric surface layer.

In the absence of thermal modelling of the upper lake layer in the current simulation, calculated evaporation rates should be regarded as approximations. Further improvement in future studies can be obtained if initial profiles of moisture and temperature are

available for the model initialization. The specific humidity profiles over the centre of the lake as obtained following the model dynamic initialization (namely at the beginning of the simulations) are given in Table 3.

TABLE 3. SPECIFIC HUMIDITY (g kg^{-1}) AT THE CENTRE OF THE LAKE FOR 2000 AS OBTAINED FOLLOWING THE MODEL DYNAMICAL INITIALIZATION (GIVEN IN THE LOWER MODEL LEVELS).

	Level (m)										
	5	15	50	100	300	500	700	900	1200	1500	2000
Summer day ($T_s = 33$ °C)	14·0	13·9	13·9	13·8	13·6	13·5	13·3	13·0	12·9	11·2	7·1
Winter day	5·3	5·2	5·0	4·7	4·3	4·0	3·8	3·4	2·9	2·3	1·7

5. CONCLUSION

Numerical model simulations have been carried out for the investigation of selected meteorological patterns over the Dead Sea, associated with two typical synoptic situations. Additionally, general aspects of a combined lake–mountain circulation have been discussed. The summer case, which is the most common situation, has been emphasized.

From the applied point of view, based on the state of the art of numerical modelling, the study provides some insight into the meteorological patterns in the Dead Sea region. While the current simulations are preliminary, the partial verification analysis suggests that further improvement of the results will require use of a 3D fine grid over the Dead Sea region.

The effect of external flows (synoptic or mesoscale) was shown to shift the LMC significantly towards the windward shore during day-light hours, consequently creating an emphasized circulation cell over most of the lake but with a diminished circulation over the downwind shore. The relation between the slope steepness and the lake water temperature (or the thermal stratification over the lake) has been investigated, indicating the possible reduction in the LMC near the lake, as surface water temperature decreases. In addition, for a given stable thermal stratification over the lake, as the terrain slopes become steeper, there is a tendency for a weaker LMC.

ACKNOWLEDGMENT

Acknowledgment is made to the Bi-National Israel–United States Science Foundation and, the Atmospheric Sciences Section of the National Science Foundation (Grant ATM-8242931) for their support in undertaking this research. Computer simulations presented in this study were performed at the National Center for Atmospheric Research which is supported by the National Science Foundation. We would like to thank Professor A. Katz, Drs M. Weiss and I. Steinhorn for providing us with their data and suggestions. We wish also to thank Sara Rumley and Ann Gaynor for their excellent editing and typing.

REFERENCES

Alpert, P. 1980 *A mesometeorological model with topography.* Ph.D. thesis, Dept, of Atmospheric Sciences, The Hebrew University, Jerusalem.

Anthes, R. A. 1978 The height of the planetary boundary layer and the production of circulation in a sea breeze model. *J. Atm. Sci.*, **35**, 1237–1239.

Ashbel, D. 1939 The influence of the Dead Sea on the climate of its neighbourhood. *Quart. J. R. Met. Soc.*, **65**, 185–194.

Atlas of Israel 1970 Chapter 3/IV, Survey of Israel, Ministry of Labour, Jerusalem.

Bitan, A. 1974 The wind regime in the north-west section of the Dead Sea. *Arch. Meteor. Geoph. Biokl., Ser. B*, **22**, 313–335.

1977 The influence of the special shape of the Dead Sea and its environment on the local wind system. *ibid*, **24**, 283–301.

Carpenter, K. M.	1979	An experimental forecast using a non-hydrostatic mesoscale model. *Quart. J. R. Met. Soc.*, **105**, 629–655.
Dalu, G. A.	1978	A parametrization of heat convection for a numerical sea breeze model. *ibid*, **104**, 797–807.
Doron, E.	1979	Objective analysis of mesoscale flow fields and trajectory calculation. *Israel J. Earth Sci.*, **28**, 33–41.
Estoque, M. A. and Gross, J. M.	1981	Further studies of lake breeze. Part II: theoretical study. *Mon. Wea. Rev.*, **109**, 619–634.
Jaffe, S.	1976	*Summer climate in Israel*, Ser. E., No. 30, Israel Meteorological Service, Bet-Dagan.
Johnson, A. and O'Brien, J.	1973	A study of an Oregon sea-breeze event. *J. App. Meteor.*, **12**, 1267 1283.
Krauss, E. B.	1972	*Atmosphere–ocean interaction*, Clarendon press, Oxford.
Levi, M.	1967	Fog in Israel. *Israel J. Earth Sci.*, **16**, 2–21.
MacPherson, A. K. and Kelly, R. E.	1976	A horizontal telescoping grid with a vertical nested layer using bi-cubic splines. *Mon. Wea. Rev.*, **104**, 932–941.
Mahrer, Y. and Pielke, R. A.	1976	A numerical study of the air flow over Barbados. *ibid*, 1392–1402.
	1977	A numerical study of the air flow over irregular terrain. *Contr. Atm. Phys.*, **50**, 98–113.
	1978	A test of an upstream spline interpolation technique for the advective terms in a numerical mesoscale model. *Mon. Wea. Rev.*, **106**, 818–830.
Mahrer, Y. and Segal, M.	1979	A numerical study of the air flow over Israel using a two-dimensional mesoscale model. *Preprints, 4th Conference on Numerical Weather Prediction.* Amer. Meteor. Soc., 256–258.
Mizzi, A. P.	1982	*A coupled sea breeze and coastal upwelling model.* M.Sc. thesis, Dept, of Environmental Sciences, University of Virginia.
Moroz, W. J.	1967	A lake breeze on the eastern shore of lake Michigan: observation and model. *J. Atm. Sci.*, **103**, 474-485.
Neev, D. and Emery, K. O.	1967	*The Dead Sea.* Israel Geo. Sur. Bull., No. 41.
Neumann, J. and Mahrer, Y.	1975	A theoretical study of the lake and land breezes of circular lakes. *Mon. Wea. Rev.*, **103**, 474–485.
Ookouchi, Y., Uryu, M. and Sawada, R.	1978	A numerical study of the effects of mountains on the land and sea breezes. *J. Met. Soc. Japan*, **56**, 368–385.
Physick, W. L.	1976	A numerical model of the sea breeze phenomenon over lake or gulf. **33**, 2107–2135.
Pielke, R. A.	1974	A three dimensional numerical model of the sea-breezes over south Florida. *Mon. Wea. Rev.*, **102**, 115–139.
Pielke, R. A. and Martin, C. L.	1981	The derivation of a terrain-following coordinate system for the use in hydrostatic model. *J. Atm. Sci.*, **38**, 1707–1713.
Segal, M., Mahrer, Y. and Pielke, R. A.	1982a	Numerical study of wind energy characteristics over heterogeneous terrain – central Israel case study. *Bound.-Layer Meteor.*, **22**, 373–392.
	1982b	*A three dimensional numerical model study of summer meteorological patterns over the southern coasts of the Mediterranean Sea.* First International Conference on Meteorology and Air/Sea Interaction of the Coastal Zone, The Hague, May 10–14.
Shaia, J.	1962	*Upper air data for Be'er-Ya'aqov.* Meteor. Notes. Ser. A, No. 19. Israel Meteorological Service.
Skibin, D. and Hod, A.	1979	Subjective analysis of mesoscale flow patterns in northern Israel. *J. App. Meteor.*, **19**, 329–338.
Weiner, D.	1980	The Mediterranean–Dead Sea project: a mathematical model and dynamic optimization of a solar hydroelectric power plant. *J. Solar Energy Eng.*, **102**, 281–286.
Wippermann, F.	1981	The applicability of several approximations in meso-scale modelling – a linear approach. *Contr. Atm. Phys.*, **54**, 298–308.